

1 **Excited State Resonance Raman of Flavin Mononucleotide: Comparison of Theory and Experiment**

2 Dale Green,¹ Palas Roy,¹ Christopher R. Hall,^{1†} James N. Iuliano,² Garth A. Jones,¹ Andras Lukacs,³

3 Peter J. Tonge^{2*} and Stephen R. Meech^{1*}

4 ¹*School of Chemistry, University of East Anglia, Norwich NR4 7TJ, U.K.*, ²*Department of Chemistry,*

5 *Stony Brook University, Stony Brook, New York 11794-3400, United States*, ³*Department of*

6 *Biophysics, Medical School, University of Pecs, Szigeti ut 12, 7624 Pecs, Hungary*

7 **Abstract**

8 Blue light absorbing flavoproteins play important roles in a variety of photobiological processes.

9 Consequently, there have been numerous investigations of their excited state structure and dynamics,

10 in particular by time resolved vibrational spectroscopy. The isoalloxazine chromophore of the

11 flavoprotein co-factors has been studied in detail by time resolved Raman, lending it a benchmark

12 status for mode assignments in excited electronic states of large molecules. However, detailed

13 comparisons of calculated and measured spectra have proven challenging, as there are many more

14 modes calculated than are observed, and the role of resonance enhancement is difficult to

15 characterise in excited electronic states. Here we employ a recently developed approach due to Elles

16 and co-workers. (*J. Phys. Chem. A* **2018**, *122*, 8308–8319) for the calculation of resonance enhanced

17 Raman spectra of excited states, and apply it to the lowest singlet and triplet excited states of the

18 isoalloxazine chromophore. There is generally good agreement between calculated and observed

19 enhancements, which allows assignment of vibrational bands of the flavoprotein co-factors to be

20 refined. However, some prominently enhanced bands are found to be absent from the calculations,

21 suggesting the need for further development of the theory.

22 *Address for correspondence: peter.tonge@stonybrook.edu; s.meech@uea.ac.uk

23 [†]Present address: School of Chemistry, 153, The University of Melbourne, Masson Rd, Parkville VIC

24 3052, Australia

25 **Introduction**

26 Flavoproteins play a key role in biochemistry because the flavin cofactor can access a range of
27 oxidation and protonation states, allowing the proteins to participate in a variety of redox reactions.¹
28 The co-factor (Flavin Mononucleotide, FMN, or Flavin Adenine Dinucleotide, FAD) gives these proteins
29 their yellow colour, which arises from their common isoalloxazine chromophore, which absorbs at
30 around 450 nm. Over the past thirty years a number of flavoproteins have been shown to play an
31 important role in photobiology.²⁻³ Three families of photoactive flavoproteins have been identified,
32 the blue light using flavin (BLUF) domain proteins,⁴ the light-oxygen-voltage (LOV) domain proteins⁵⁻⁷
33 and the photolyase/cryptochromes.⁸ These are the light sensing elements in an array of
34 photobiological functions, playing a role in processes ranging from phototaxis to circadian rhythms.
35 Several photoactive flavoproteins function by controlling gene expression in response to light, a
36 property which has recently been recruited in optogenetics applications.⁹

37 The obvious importance of isoalloxazine excited state chemistry has stimulated a number of
38 investigations. Both optical and infra-red spectroscopy have been applied to probe flavin
39 photochemistry in all of its accessible charge states.¹⁰⁻¹³ These studies have been extended to
40 photoactive flavoproteins, and the effects of optical excitation on their structure and excited state
41 dynamics have been investigated by crystallography, NMR and pump-probe spectroscopy
42 respectively.¹⁴⁻²² These experiments have been complemented by quantum chemical calculations.²³⁻²⁷
43 Time resolved infra-red (TRIR) spectroscopy in particular has proven a useful probe of flavin excited
44 state reactions, and their effect on the surrounding protein matrix.²⁸⁻³⁴ However, TRIR measurements
45 of flavoproteins have significant drawbacks. First, measurements must be made in D₂O buffer, as H₂O
46 absorbs strongly in the characteristic protein amide and sideband region. Second, it cannot be applied
47 to large complexes, due to strong absorption by amide modes. Finally, TRIR difference spectra are
48 often complicated and difficult to interpret, involving contributions from both the chromophore and
49 the surrounding protein matrix.³⁵

50 In contrast, transient Raman spectroscopy can be applied in aqueous solutions and to proteins of any
51 size, limited only by their solubility. Further, resonance enhancements can be exploited, yielding
52 simpler state specific vibrational data. However, the application of Raman in time resolved
53 photobiology has been restricted by the twin problems of strong background fluorescence and the
54 weakness of the signal that can be generated from transient states. These problems can to a large
55 extent be overcome by femtosecond stimulated Raman spectroscopy (FSRS). FSRS is a coherent
56 multipulse experiment which yields well resolved Raman spectra of resonant excited states with good
57 signal to noise and ultrafast (sub 100 fs) time resolution. The FSRS experiment has been described in
58 detail elsewhere.³⁶⁻³⁷

59 Weigel and co-workers reported the first FSRS spectrum of the singlet excited states of solutions of
60 riboflavin and FAD.³⁸ They assigned the observed excited state Raman spectra with the aid of TDDFT
61 calculations, and contrasted them with ground state measurements. Hall and co-workers extended
62 the FSRS method to probe FAD in photoactive flavoproteins, and showed that the excited state spectra
63 were sensitive to the protein environment.³⁹ Recently, two further FSRS studies have investigated
64 excited states of FMN. Andrikopoulos et al probed singlet and triplet states of FMN in solution, and
65 assigned them on the basis of TDDFT calculation.⁴⁰ Iuliano et al also reported singlet and triplet state
66 FSRS, and presented a detailed assignment based on the study of a series of FMN isotopologues, both
67 experimentally and through TDDFT, in solution and in LOV domain proteins.⁴¹ As a result of these quite
68 extensive studies, the chromophore of the flavoproteins, isoalloxazine, has one of the best
69 characterised excited state spectra, giving it the status of a benchmark for assignment of excited state
70 vibrations of large molecules, in addition to its established role in photobiology.

71 The experimental FSRS spectra of S₁ and T₁ isoalloxazines map well onto the results of TDDFT
72 calculations. However, many more modes are found in the calculated spectrum than appear in the
73 experiment. Typically, only five or six bands appear in the FSRS spectrum measured in the fingerprint
74 (1100 – 1800 cm⁻¹) region of isoalloxazine, and in many cases these can plausibly be assigned to several
75 different nearby calculated modes.^{38, 40-41} With the aid of spectra from isotopologues it proved possible

76 to assign some experimental bands to specific modes, but in other cases multiple possible assignments
77 remained.⁴¹ The reason for the relative simplicity of the FSRS spectrum, compared to the calculation,
78 is that FSRS is resonantly enhanced. It is well established that resonance enhancements simplify
79 ground state Raman spectra, as has also been shown for isoalloxazines.⁴²⁻⁴³ The challenge with excited
80 state resonant FSRS spectra is that while the spectra represent the lowest excited states of most
81 interest (S_1, T_1) the factors controlling the enhancement rests with the properties of the upper ($S_n, T_n,$
82 $n>1$) states. Recently Elles and co-workers established that this can play a major role in FSRS spectra,
83 and made important progress in developing and testing methods for calculating resonance enhanced
84 FSRS.⁴⁴⁻⁴⁵ Given the importance of the flavin co-factors in photobiology, and the benchmark status of
85 isoalloxazine emerging from the multiple observations of its excited state Raman spectra, we have
86 applied the approach described by Elles to model the FSRS of S_1 and T_1 isoalloxazine.

87 **Theory**

88 Strong enhancement of a mode in a resonance Raman spectrum is a result of the equilibrium geometry
89 of the resonant, upper, electronic state, $|N\rangle$, being displaced with respect to that of the lower
90 electronic state, $|I\rangle$.⁴⁶ This gives rise to significant wavefunction overlap in the Franck-Condon factors
91 $\langle v_f | v_n \rangle$ and $\langle v_n | v_i \rangle$, between the vibrational levels of the upper state, $|v_n\rangle$, and the initial and final
92 vibrational levels of the lower electronic state, $|v_i\rangle$ and $|v_f\rangle$. As described by Elles *et al.*, the intensity
93 of the k th mode of the lower electronic state, I_k , is proportional to the square of its polarizability
94 tensor, α_{fi}^k , which can be determined using the semiclassical gradient approximation.⁴⁴ This accounts
95 for the vibrational overlap by propagating an initially Gaussian wavepacket on the potential energy
96 surface of the upper electronic state, V_N , using classical equations of motion.⁴⁷⁻⁵⁰ To first order, the
97 evolution of the wavepacket is thus dictated by the gradient of the upper state potential with respect
98 to the vibrational coordinate of the lower electronic state, which increases with greater displacement
99 of the equilibrium geometry of V_N .

100
$$I_k \propto \omega_p (\omega_p - \omega_k)^3 |\alpha_{fi}^k|^2 \approx \omega_p (\omega_p - \omega_k)^3 \frac{|\mu_{NI}|^4}{2\omega_k} \left(\frac{\partial V_N}{\partial q_k} \right)^2,$$

101 where ω_k is the mode frequency, q_k is the normalised mode coordinate, ω_p is the excitation (pump)
 102 frequency and μ_{NI} is the electric transition dipole moment between the lower and upper electronic
 103 state.⁴⁵ The resonance Raman intensity is therefore also strongly dependent on the oscillator strength
 104 of the electronic transition, $f \propto E_p |\mu_{NI}|^2$ where $E_p = \hbar\omega_p$.⁴⁴

105 The Condon approximation for the electric transition dipole moment restricts the gradient
 106 approximation to the Albrecht A term in the theory of Raman scattering, neglecting any Herzberg-
 107 Teller vibronic coupling between electronic states involved in the higher (B, C, D) terms.⁵¹ These terms
 108 are expected to have a greater contribution in excited state resonance Raman spectra, where the
 109 increased density of states reduces the separation energies. In this format, the gradient approximation
 110 is limited to resonance with a single electronic state, neglecting any mode enhancement due to the
 111 additive effects of resonance with nearby excited states. Similarly, this approach does not account for
 112 quantum interference caused by allowed transitions to multiple electronic states or population
 113 transfer due to nonadiabatic coupling between states, which result in resonance de-enhancement.⁵²

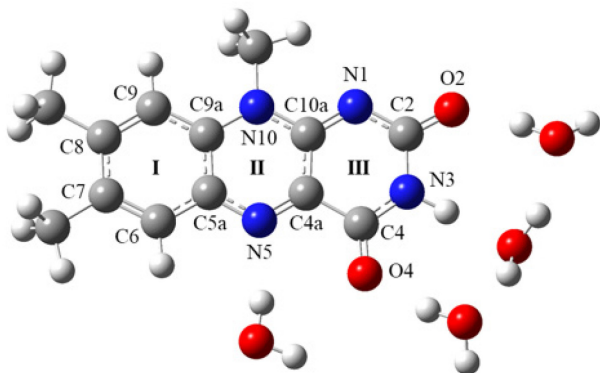
114 ⁵³ Reduced enhancement due to homogeneous broadening, most significant for low frequency modes,
 115 is also neglected in this approach.^{45, 54-55}

116 **Methods**

117 *(i) Femtosecond Stimulated Raman* The experimental FSRS spectra we aim to simulate were measured
 118 previously⁴¹ using an instrument described in detail elsewhere.⁵⁶⁻⁵⁷ The narrowband (ca. 10 cm⁻¹)
 119 picosecond ‘Raman Pump’ pulses was centered at 750 nm to be resonant with the known excited state
 120 transient absorption of FAD.⁴⁰ The excitation was at 450 nm, generated from the OPA (Topas Prime).

121 *(ii) Off-resonance Raman Calculations.* The optimized structures and off-resonance Raman spectra
 122 were calculated as described in our previous paper (see also supporting information).⁴¹ All calculations
 123 were completed using Gaussian 16.⁵⁸ The ribityl-5'-phosphate in FMN was replaced with a methyl

124 group for most calculations, thus modelling the isoalloxazine chromophore in FMN as lumiflavin. The
 125 lumiflavin was solvated by four explicit water molecules³⁸ as well as a polarizable continuum model
 126 (PCM)⁵⁹⁻⁶⁰ for water. The optimized structure of the ground electronic state, S_0 , was obtained using
 127 DFT at the B3LYP⁶¹⁻⁶²/TZVP⁶³ level of theory and is presented in figure 1, showing the arrangement of
 128 water molecules around the polar end of isoalloxazine. This level of theory was chosen to align with
 129 our earlier work, and because the functional is well established and benchmarked for frequency
 130 calculations. The four water molecules represent the H-bonding interaction, which causes a red-shift
 131 of $\pi\pi^*$ and a blue-shift of $\pi\pi^*$ transitions such that $S_0 \rightarrow S_1$ corresponds to an allowed $\pi\pi^*$ transition.³⁸
 132⁶⁴⁻⁶⁵ The orientation of the water molecules lowers the symmetry from the C_s to C_1 point group. The
 133 excited state geometries were optimized using TD-DFT for S_1 and unrestricted DFT for T_1 at the same
 134 level of theory and solvation used for the ground state. The three optimized structures were
 135 characterised using harmonic frequency analysis at 298.15 K and 1 atm, identifying genuine minima
 136 and yielding off-resonance Raman spectra for each of S_0 , S_1 , and T_1 .



137
 138 **Figure 1:** Optimized geometry of lumiflavin in the ground electronic state (S_0) with atomic labels, obtained using
 139 B3LYP/TZVP level of theory solvated by four water molecules as well as a PCM.

140 *(iii) Resonance Raman Calculations.* Resonance Raman spectra for each of S_0 , S_1 , and T_1 are calculated
 141 using the gradient approximation method as described for FSRS by Elles *et al.*⁴⁴⁻⁴⁵ TD-DFT calculations
 142 are repeated for several steps along each vibrational mode coordinate of the lower state, S_i or T_i ,
 143 including the optimised geometry, providing the potential energy surfaces of the upper excited states,
 144 S_N or T_N , in this region. The potential energy surfaces are then fit with a polynomial function and
 145 differentiated to evaluate the gradients of the upper states at the optimised geometry of the lower

146 state, as required for equation 1. Here, TD-DFT was performed for five steps along the normalized
147 mode coordinate, $q_k = 0, \pm 0.1, \pm 0.2$, for all modes in the range 1150 - 1750 cm⁻¹ (31 modes for each
148 of the ground excited singlet and triplet states) for and the potential energy surfaces were accurately
149 fit with a cubic function to account for the anharmonicity implicit to TD-DFT (see supporting
150 information). The appropriate upper excited state to be used in equation 1 corresponds to the
151 transition approaching resonance with the excitation wavelength which has the greatest oscillator
152 strength, as discussed below. Transition dipole moments between excited singlet states are obtained
153 from the TD-DFT results at the optimized geometry of S₁ using the Multiwfn program.⁶⁶

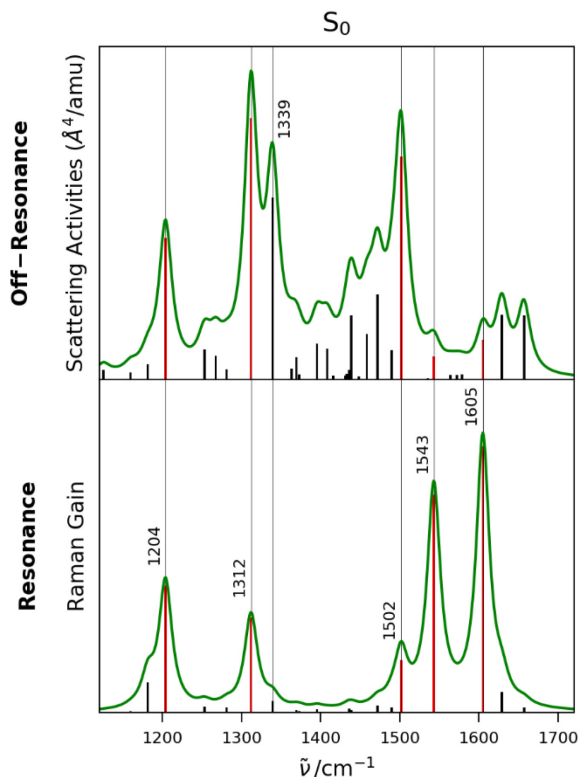
154 As discussed by Elles *et al.*, this method is limited by the inability of TD-DFT to account for double-
155 excitation character of electronic states, which may be overcome by using alternative methods such
156 as equation-of-motion coupled-cluster theory with single and double excitations (EOM-CCSD).⁴⁴
157 Significant double-excitation character is expected for higher excited states populated by the
158 sequential absorption of two photons, such as the resonant singlet states, S_N. However, the rapid
159 scaling in computational cost with increasing system size for coupled-cluster methods warrants less
160 demanding TD-DFT for studies involving repeated calculation for larger molecules, such as
161 lumiflavin.⁶⁷⁻⁶⁹

162 **Results and Discussion**

163 In our previous paper, transitions in the FSRS spectra of the S₁ and T₁ excited states of FMN were
164 assigned through comparison of the shifts observed for a series of isotopologues with shifts in the
165 calculated off-resonance Raman spectra. However, as off-resonance spectra neglect the enhancement
166 due to the gradient of the resonant state involved in FSRS, the assignments were based primarily on
167 the calculated mode frequencies, and the observed peaks are often associated with several calculated
168 modes. The transient absorption spectra of FMN at early times show a broad S₁→S_n excited state
169 absorption band from ca. 700 - 900 nm which probably involves multiple excited singlet states. At later
170 times a more intense T₁→T_n band is observed at 712 nm, which is pre-resonant with the 750 nm

171 excitation wavelength, leading to significant resonance enhancement.⁴⁰ Calculation of the resonance
172 Raman spectra using the gradient approximation method described above should therefore enable an
173 improved assignment of the S₁ and T₁ FSRS peaks, by accounting for the enhancement due to the
174 resonant singlet and triplet states. First, the model is benchmarked against the well-known resonance
175 Raman spectrum for the ground electronic state (S₀) of isoalloxazine, and then applied to calculate
176 resonance Raman spectra for the excited states S₁ and T₁, which are then used to refine the
177 assignment of the measured FSRS peaks.

178 (i) *S₀ Benchmark.* Calculated off-resonance and resonance Raman spectra for the ground state, S₀, are
179 presented in figure 2. The calculated frequencies for S₀ include an empirical scaling factor of 0.965
180 commonly used for this level of theory and basis set.⁷⁰ The ground state resonance Raman spectra
181 reported for both riboflavin⁴²⁻⁴³ and lumiflavin⁷¹ show excellent agreement with the calculated
182 spectrum. The resonance Raman spectrum of riboflavin reported by Kitagawa *et al.* identifies five
183 strongly enhanced modes at 1252, 1355, 1407, 1584 and 1631 cm⁻¹,⁴² which correspond to transitions
184 at 1204, 1312, 1543 and 1605 cm⁻¹ in the calculated spectrum. However, no enhancement was
185 calculated at 1407 cm⁻¹ while a calculated enhancement at 1502 cm⁻¹ has no experimental
186 counterpart. The missing enhancement at 1407 cm⁻¹ is similarly weak when calculated using the
187 independent mode, displaced harmonic oscillator (IMDHO) model, as reported by Weigel *et al.*³⁸ and
188 Kar *et al.*⁷¹ IMDHO uses the same time-dependent theory as the semiclassical gradient approximation
189 described above, but assumes the excited state potential energy surfaces are harmonic.⁷²



190 **Figure 2:** Calculated off-Resonance and Resonance Raman spectra for S_0 of lumiflavin solvated by four water
 191 molecules. Resonance enhanced modes are highlighted in red.

192

193 The resonance Raman spectrum in figure 2 is calculated using the gradient of the S_1 potential energy
 194 surface at the optimised geometry of S_0 , with an excitation wavelength of 488 nm to match the
 195 literature. The calculated spectra are broadened by a Lorentzian function with FWHM of 20 cm^{-1} and
 196 scaled so that the original 'stick' spectra are contained within the lineshape. The five modes with the
 197 strongest enhancement in the resonance Raman spectrum are assigned in Table 1 and highlighted in
 198 red in Figure 2. Modes are numbered according to the output of the frequency analysis at the
 199 optimised geometry for each electronic state. The numbering of modes for S_0 in Table 1 is therefore
 200 independent of the numbering for S_1 and T_1 modes discussed later. The assignment of these modes
 201 agrees with that of Weigel *et al.* using the IMDHO model, as well as the displacements identified
 202 through isotopic frequency shifts by Kitigawa *et al.*^{38, 42}

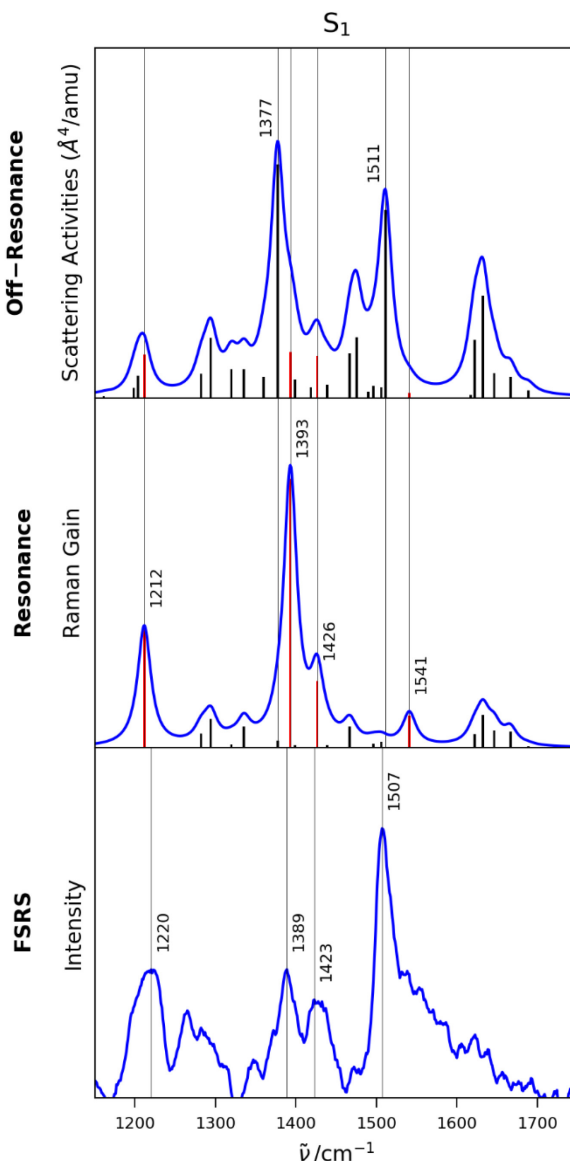
203

Experimental ⁴² /cm ⁻¹	Calculated /cm ⁻¹	Mode	Assignment
1252	1204	75	<i>as</i> C2-N3-C4, <i>s</i> C7-Me, <i>s</i> C8-Me, <i>w</i> C6-H, <i>w</i> C9-H
1355	1312	79	<i>as</i> N10-C10a-C4a, <i>ss</i> C2-N3-C4, <i>as</i> C5a-C9a-C9, <i>s</i> C7-C8, <i>w</i> C6-H
-	1502	95	<i>as</i> N10-C10a-N1, <i>s</i> C4a-N5, <i>ss</i> C8-C9-C9a, <i>ss</i> (C2=O2, C4=O4), <i>w</i> N3-H, <i>b</i> N10-Me
1584	1543	97	<i>s</i> C5a-C9a, <i>as</i> C7-C8-C9, <i>as</i> N5-C4a-C10a
1631	1605	101	<i>s</i> C4a-N5, <i>s</i> C6-C7, <i>s</i> C9-C9a, <i>s</i> C2=O2

204 **Table 1:** Assignment of resonance enhanced modes for S_0 . *s*: stretch, *a*-: antisymmetric, *s*-: symmetric, *w*: wag,
205 *b*: bend. Three atom stretches are described with respect to the centre atom and delocalised/coupled carbonyl
206 stretches are indicated using brackets.

207 The resonance enhanced modes at 1204 cm^{-1} , 1312 cm^{-1} and 1502 cm^{-1} also produce intense peaks in
208 the off-resonance Raman spectrum, in contrast to the most enhanced modes at 1543 cm^{-1} and
209 1605 cm^{-1} . The intense peak in the off-resonance Raman spectrum at 1339 cm^{-1} shows minimal
210 enhancement in the resonance Raman spectrum. The carbonyl stretches at 1629 cm^{-1} and 1657 cm^{-1}
211 also show very little enhancement in the resonance Raman spectrum, reflecting the negligible
212 displacement between the potential minima for S_1 and S_0 for these modes. All five modes in Table 1
213 feature strong C-N as well as ring I stretches such that the vibrations are delocalised across the
214 isoalloxazine moiety.

215 (ii) S_1 Assignment. The calculated off-resonance and resonance Raman spectra for S_1 are shown in
216 figure 3. The modes with the greatest resonance enhancement are again highlighted in red to
217 emphasise the contrast with off-resonance intensities. The previously reported⁴¹ FSRS spectrum for S_1
218 is also shown in figure 3. Recognizing the dominance of the transition dipole moment in equation 1,
219 $\propto |\mu_{NI}|^4$, the resonance Raman spectrum is calculated using the gradient of S_8 for the upper state, as
220 the TD-DFT results identify $S_1 \rightarrow S_8$ has the greatest oscillator strength of transitions in the region of
221 the 750 nm Raman pump wavelength. The energies and oscillator strengths of neighbouring
222 transitions are provided in the supplementary information. The assignment of each peak in the FSRS
223 spectrum of S_1 is given in table 2, including the modes identified in our previous work using isotopic
224 frequency shifts in off-resonance spectra, as well as the refinements now proposed by the calculated
225 resonance Raman spectrum.



226
227
228
229

Figure 3: Calculated off-Resonance and Resonance Raman spectra for S_1 of lumiflavin solvated by four water molecules, as well as measured FSRS spectrum for S_1 of FMN in H_2O from ref⁴¹. Resonance enhanced modes are highlighted in red.

230
231
232
233
234
235
236
237
238

FSRS /cm ⁻¹	Off-Resonance Raman /cm ⁻¹	Resonance Raman /cm ⁻¹	Mode	Assignment
1220	1198	1212	73	sN5-C5a, sN3-C4, sC6-C7, wC6-H, wC9-H
	1204		74	sC2-N3, ssN5-C4a-C10a, sC9-C9a, sC6-C7, wC6-H, wC9-H, wN10-Me
	1212		75	asC10a-N1-C2, sN3-C4, sC4a-N5, sC6-C7
1389	1360	1393	80	sN10-C10a, sN3-C4, asC7-C8-C9, asC6-C5a-C9a, bN10-Me, bC7-Me, bC8-Me
	1377		81	sC4a-C10a, sN1-C2, sC5a-C9a, sC6-C7, wC6-H
	1393		82	sC4a-N5, sN10-C10a, sN1-C2, ssC8-C9-C9a, wC6-H, bN10-Me, wC8-Me, wC7-Me
1423	1426	1426	85	asN5-C4a-C4, ssC10a-N1-C2, sN3-C4, wC6-H, scC8-Me, scN10-Me
1507	1511		95	sC4a-N5, sN1-C10a, sC7-C8, sC5a-C9a, wN3-H, bC7-Me, bC8-Me, bN10-Me, wC9-H, wC6-H

239 **Table 2:** Assignment of FSRS peaks for S_1 based on the calculated off-resonance and resonance Raman spectra.
240 s: stretch, a: antisymmetric, s: symmetric, w: wag, sc: scissor, b: bend. Three atom stretches are described with
241 respect to the centre atom.

242 The off-resonance Raman spectrum associates the FSRS peak at 1220 cm⁻¹ with a cluster of ring modes
243 73, 74 and 75. The isolated enhancement of mode 75 at 1212 cm⁻¹ in the resonance Raman spectrum
244 now refines this assignment. Similarly, ¹⁵N or ¹³C substitution resulted in a red-shift of the FSRS peak
245 at 1389 cm⁻¹ which was also shown by modes 80, 81 and 82, where mode 81 at 1377 cm⁻¹ has the
246 greatest intensity in the off-resonance spectrum, but mode 82 best reproduced the red-shifts of the
247 FSRS peak. The resonance Raman spectrum shows negligible enhancement of mode 81, in favour of
248 significant enhancement of mode 82 at 1393 cm⁻¹. The 1389 cm⁻¹ peak is therefore assigned to mode
249 82 which features strong C-N and ring I stretches, as observed for the enhanced ground state
250 vibrations, whereas the greatest displacements involved in mode 81 are localised on ring II; calculated
251 mode displacements are shown in the supplementary information. The resonance Raman spectrum
252 confirms the assignment of the FSRS peak at 1423 cm⁻¹ to mode 85 at 1426 cm⁻¹. However, the FSRS
253 peak at 1507 cm⁻¹ has no clear assignment in the calculated resonance Raman spectrum. The peak at
254 1507 cm⁻¹ shows twice the amplitude of the other FSRS peaks and was insensitive to ¹⁵N or ¹³C

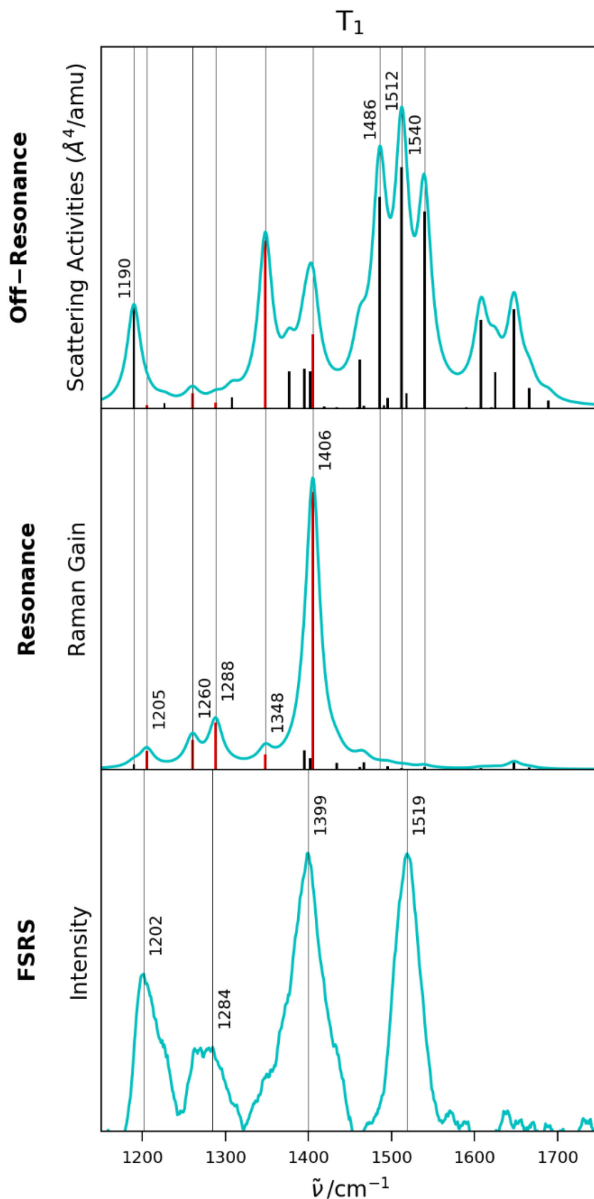
255 substitution and D₂O exchange. Despite the intensity of mode 95 at 1511 cm⁻¹ in the off-resonance
256 spectrum, this mode shows no enhancement in the resonance Raman spectrum. Similarly, the small
257 enhancement of mode 96 at 1541 cm⁻¹ does not account for the dominance of the 1507 cm⁻¹ peak in
258 the FSRS spectrum, though it may contribute to the shoulder to higher wavenumber of the peak (figure
259 3).

260 The difficulties in assigning the 1507 cm⁻¹ peak must therefore result from the limitations of the
261 gradient approximation, which does not account for vibronic coupling between electronic states, or
262 the density of excited states. The neglect of vibronic coupling means that overtones and combination
263 bands are not resolved in the resonance Raman spectra calculated using this method. The absence of
264 a fundamental mode enhancement at ca. 1500 cm⁻¹ therefore suggests consideration of a possible
265 assignment of the 1507 cm⁻¹ FSRS peak to an overtone or combination of lower frequency modes. In
266 the limit of strong damping, typical for large molecules in the condensed phase, the intensities of
267 overtones and combination bands are also determined by the displacement of the upper state
268 potential energy surface, but cannot exceed the intensities of the fundamental peaks for the
269 contributing modes.^{46, 73} This was demonstrated by Quincy *et al.* for a combination band of
270 diphenylthiophene, where the fundamental peaks of the contributing modes are clearly visible at
271 lower frequency in the FSRS spectrum, and are significantly (> 6 times) more intense.⁴⁴ However,
272 extension of the calculated resonance Raman spectra for S₁ isoalloxazine to the lower frequency 400
273 - 900 cm⁻¹ region identified no modes that exceeded, or even matched, the intensity of the peaks in
274 figure 3. Thus an assignment to an overtone or combination band is not supported.

275 Strong peaks at ca. 1500 cm⁻¹ were also observed in the FSRS spectra of S₁ reported by Weigel *et al.*
276 and Andrikopoulos *et al.*, and assigned using off-resonance calculations.^{38, 40} However, Andrikopoulos
277 *et al.* reported that the assignment of this strong peak had the greatest difference between calculated
278 and experimental frequencies; these complications are consistent with the present difficulties.⁴⁰ If the
279 peak at 1507 cm⁻¹ is indeed the result of a separate vibrational mode, the missing enhancement must
280 also reflect the limitations of TD-DFT in describing the higher excited singlet states.

281 Another possibility is a role for a different enhancing transition, although the order of magnitude
282 decrease in oscillator strength for transitions to states neighbouring S_8 suggests the density of
283 electronic states is not the primary issue (supporting information). Even so this possibility was
284 investigated. There is also no strong enhancement at ca. 1500 cm^{-1} in resonance Raman spectra
285 calculated using S_6 and S_7 as alternative near resonant states, so this is also not a plausible explanation
286 (supporting information).

287 *(iii) T_1 Assignment.* The calculated off-resonance and resonance Raman spectra for T_1 are shown in
288 figure 4, along with the previously reported FSRS spectrum of T_1 recorded 3 ns after electronic
289 excitation to allow for intersystem crossing.⁴¹ The resonance Raman spectrum is calculated using the
290 gradient of T_5 for the upper state, selected as the oscillator strength of the $T_1 \rightarrow T_5$ transition is two
291 orders of magnitude greater than $T_1 \rightarrow T_4$, although the transition energy is further from resonance
292 with the 750 nm Raman pump wavelength; see supplementary information. This is in line with the
293 dominant role of transition dipole moment in the enhancement. Assignments of the FSRS peaks for
294 T_1 are given in table 3.



295

296 **Figure 4:** Calculated off-Resonance and Resonance Raman spectra for T_1 of lumiflavin solvated by four water
 297 molecules, as well as measured FSRS spectrum for T_1 of FMN in H_2O from ref. ⁴¹ Resonance enhanced modes are
 298 highlighted in red.

299

300

301

302

303

304

305

FSRS /cm ⁻¹	Off-Resonance Raman /cm ⁻¹	Resonance Raman /cm ⁻¹	Mode	Assignment
1202	1190	1205	73	<i>as</i> N1-C2-N3, <i>as</i> C4-C4a-C10a, <i>as</i> C5a-C6-C7, wC6-H, ssC8-C9-C9a
			74	sN3-C4, sC5a-N5, sC9-C9a, wC6-H, wC9-H, wN10-Me
1284	1260	1260	76	<i>as</i> C2-N3-C4, sN10-C10a, sC4a-N5, sC6-C7, wC6-H, wN10-Me
		1288	77	sC7-Me, sC5a-N5, sN10-Me, sN1-C2, wC6-H, wC9-H
1399	1348	1406	79	sN10-Me, sN1-C10a, ssC2-N3-C4, <i>as</i> C6-C7-C8, <i>as</i> C9-C9a-C5a, wC6-H, wC9-H
	1395		81	sN1-C10a, sC4a-N5, ssC2-N3-C4, sC9-C9a, bC7-Me, wN3-H
	1406		83	sN10-C10a, sC4a-N5, sN1-C2, sN3-C4, ssC8-C9-C9a, wC7-Me, wC8-Me, wN10-Me
1519	1486		90	sC4a-N5, sN1-C10a, <i>as</i> (C2=O2, C4=O4), wN3-H
	1512		94	sC4a-N5, sN1-C10a, ssC5a-C6-C7, sC8-Me, sC9a-N10, wN3-H, bN10-Me, bC7-Me
	1540		96	sC4a-N5, sN1-C10a, sC2=O2, sN3-C4, ssC7-C8-C9, wC6-H, wC9-H, wN3-H

306 **Table 3:** Assignment of FSRS peaks for T_1 based on the calculated off-resonance and resonance Raman spectra.
307 *s*: stretch, *a*-: antisymmetric, *s*-: symmetric, *w*: wag, *b*: bend. Three atom stretches are described with respect to
308 the centre atom and delocalised/coupled carbonyl stretches are indicated using brackets.

309 The off-resonance Raman spectrum identified mode 73 at 1190 cm⁻¹ as the only candidate for the FSRS
310 peak at 1202 cm⁻¹, but the resonance Raman spectrum shows this mode has negligible enhancement
311 so this peak is in fact better assigned to mode 74 at 1205 cm⁻¹, which has the greater amplitude in the
312 resonance spectrum. Again, mode 74 is delocalised across the isoalloxazine structure whereas mode
313 73 has the strongest amplitude displacements concentrated on ring III. The resonance Raman
314 spectrum confirms the earlier assignment of the FSRS peak at 1284 cm⁻¹ to modes 76 and 77 at 1260
315 cm⁻¹ and 1288 cm⁻¹, respectively, which have minimal intensity in the off-resonance spectrum, but
316 moderate enhancement in the resonance Raman spectrum. The resonance Raman spectrum for T_1 is
317 dominated by enhancement of mode 83 at 1406 cm⁻¹. The FSRS peak at 1399 cm⁻¹ can therefore be
318 confidently assigned to mode 83, whereas the isotopic frequency shifts in the off-resonance Raman

319 spectra had previously not distinguished between modes 79, 81 or 83 as possible assignments. As was
320 found for S_1 , the lack of enhancement in the region of 1500 cm^{-1} means assignment of the FSRS peak
321 at 1519 cm^{-1} cannot be improved beyond the previous suggestions of modes 90, 94 and 96 from the
322 off-resonance Raman spectrum; none of these modes are strongly enhanced. This dramatic difference
323 in intensity between the off-resonance and resonance Raman spectra for both S_1 and T_1 demonstrates
324 that assignments based purely on off-resonance spectra may be unreliable.

325 The 1519 cm^{-1} peak showed no significant change on D_2O exchange, with modes 90 and 96 both
326 reproducing the red-shift of the FSRS peak on ^{15}N and ^{13}C substitution, but again the absence of an
327 enhancement places a question mark over this assignment. Extension of the calculated resonance
328 Raman spectrum to the lower frequency $400 - 900\text{ cm}^{-1}$ region again did not identify any modes with
329 sufficient enhancements to support assignment of the 1519 cm^{-1} peak to an overtone or combination
330 band. Therefore, the missing enhancement of this peak links with the 1507 cm^{-1} FSRS peak for S_1 ,
331 suggesting a common origin and thus endorsing the blue-shift of this mode on triplet formation, as
332 described previously by both us and Andrikopoulos *et al.*⁴⁰ Resonance Raman spectra calculated using
333 T_4 or T_6 as the resonant state show increased enhancement above 1500 cm^{-1} , including the carbonyl
334 stretching modes, but any contribution from these states is expected to be negligible due to the
335 significantly reduced oscillator strength; see supplementary information.

336 One final possible assignment for the missing $1507/1519\text{ cm}^{-1}$ bands is that our simulations are based
337 on isoalloxazine, whereas measurements were made on FMN, so potentially the side chain might
338 make a contribution. This is unexpected, as the most strongly enhanced modes are delocalized ring
339 modes, but as a check we extended the TDDFT calculation to riboflavin, which has the same side chain
340 as FMN, but does not include the phosphate group. Although some differences were found in the
341 electronic structure and the off-resonance spectrum between isoalloxazine and FMN, the overall
342 pattern of the enhancements was not modified, and in particular there were no new candidates for
343 the identity of the $1507/1519\text{ cm}^{-1}$ bands; these data are presented in the supporting information. The

344 absence of these experimentally observed modes in the calculated enhancements therefore suggests
345 some shortcoming in the methods employed here.

346 **Conclusions**

347 Resonance enhanced FSRS provides a powerful means of studying the structure of excited electronic
348 states of large molecules in complex environments. It provides data beyond anything that can be
349 gleaned from transient absorption spectroscopy. The method has recently been applied to investigate
350 the isoalloxazine moiety in solution and in photoactive flavoproteins. These studies have been
351 supported by TD-DFT calculations, but assignment of FSRS peaks based on off-resonance Raman
352 spectra is challenging because of the large number of modes, and neglects the essential contribution
353 of the resonant excited state in determining the intensities. Here, the assignment of FSRS spectra for
354 S_1 and T_1 states of FMN, previously reported by a number of groups, has been addressed through
355 calculation of excited state resonance Raman spectra, using the time-dependent gradient
356 approximation. The calculated resonance Raman spectra have confirmed or refined the assignment of
357 almost all FSRS peaks observed for FMN or riboflavin. The generally good agreement between
358 experiment and the time-dependent gradient approximation is encouraging. However, for both S_1 and
359 T_1 FMN a prominent band at ca. 1500 cm^{-1} in the FSRS spectrum was absent from the calculations.
360 This may be due to the neglect of Herzberg-Teller vibronic couplings within the gradient
361 approximation, or may also reflect the inadequacy of TD-DFT to correctly characterise the higher
362 energy, resonant excited electronic S_n/T_n states. Employing alternative excited state methods such as
363 EOM-CCSD to obtain the excited state potential energy surfaces might reduce these concerns and so
364 identify the missing mode. Furthermore, the use of a post Hartree-Fock methodology, such as MP2,
365 would account for correlation energies more accurately and therefore give a better description of the
366 molecular geometries, especially with regards to the positioning of the explicit solvent molecules.
367 Using MP2 for geometric optimizations in combination with EOM-CCSD for excited state calculations

368 should be considered for future studies, this will however be at considerable (perhaps prohibitive)
369 additional computational expense.

370

371 **Acknowledgements**

372 This study was supported by the National Science Foundation (NSF) (MCB-1817837 to PJT) and the
373 EPSRC (EP/N033647/1 EP/R042357/1, EP/J009148/1 to SRM). JNI was supported by a National
374 Institutes of Health Chemistry-Biology Interface Training Grant (T32GM092714). AL acknowledges
375 funding from EFOP-3.6.2-16-2017-00005. Calculations presented in this paper were carried out on
376 the High Performance Computing Cluster supported by the Research and Specialist Computing
377 Support service at the University of East Anglia.

378 **Supporting information.** The supporting information describes the calculated optimized geometries,
379 excited state transition energies and oscillator strengths, the resonance Raman potential energy
380 surface fitting to calculate enhancements, additional resonance Raman spectra and key vibrational
381 mode displacements. In addition, the extension to riboflavin FMN calculations is described.

382

383 REFERENCES

384 1. Massey, V., The Chemical and Biological Versatility of Riboflavin. *Biochemical Society*
385 *Transactions* **2000**, 28, 283-296.

386 2. Losi, A.; Gartner, W., The Evolution of Flavin-Binding Photoreceptors: An Ancient
387 Chromophore Serving Trendy Blue-Light Sensors. In *Annual Review of Plant Biology*, Vol 63,
388 Merchant, S. S., Ed. 2012; Vol. 63, pp 49-72.

389 3. Losi, A.; Gartner, W., Old Chromophores, New Photoactivation Paradigms, Trendy
390 Applications: Flavins in Blue Light-Sensing Photoreceptors. *Photochemistry and Photobiology* **2010**,
391 87, 491-510.

392 4. Masuda, S., Light Detection and Signal Transduction in the Bluf Photoreceptors. *Plant and*
393 *Cell Physiology* **2013**, 54, 171-179.

394 5. Croson, S.; Rajagopal, S.; Moffat, K., The Lov Domain Family: Photoresponsive Signaling
395 Modules Coupled to Diverse Output Domains[†]. *Biochemistry* **2002**, 42, 2-10.

396 6. Christie, J. M.; Swartz, T. E.; Bogomolni, R. A.; Briggs, W. R., Phototropin Lov Domains Exhibit
397 Distinct Roles in Regulating Photoreceptor Function. *Plant Journal* **2002**, 32, 205-219.

398 7. Kottke, T.; Hegemann, P.; Dick, B.; Heberle, J., The Photochemistry of the Light-, Oxygen-,
399 and Voltage-Sensitive Domains in the Algal Blue Light Receptor Phot. *Biopolymers* **2006**, 82, 373-378.

400 8. Sancar, A., Structure and Function of DNA Photolyase and Cryptochrome Blue-Light
401 Photoreceptors. *Chemical Reviews* **2003**, 103, 2203-2237.

402 9. Losi, A.; Gardner, K. H.; Moglich, A., Blue-Light Receptors for Optogenetics. *Chemical Reviews*
403 **2018**, 118, 10659-10709.

404 10. Kandori, H., Structure/Function Study of Photoreceptive Proteins by Ftir Spectroscopy.
405 *Bulletin of the Chemical Society of Japan* **2020**, 93, 904-926.

406 11. Massey, V.; Hemmerich, P., Photoreduction of Flavoproteins and Other Biological
407 Compounds Catalyzed by De-Aza-Flavins. *Biochemistry* **1978**, 17, 9-16.

408 12. Abe, M.; Kyogoku, Y.; Kitagawa, T.; Kawano, K.; Ohishi, N.; Takaisuzuki, A.; Yagi, K., Infrared-
409 Spectra and Molecular Association of Lumiflavin and Riboflavin Derivatives. *Spectrochimica Acta Part*
410 *a-Molecular and Biomolecular Spectroscopy* **1986**, 42, 1059-1068.

411 13. Unno, M.; Sano, R.; Masuda, S.; Ono, T. A.; Yamauchi, S., Light-Induced Structural Changes in
412 the Active Site of the Bluf Domain in Appa by Raman Spectroscopy. *Journal of Physical Chemistry B*
413 **2005**, 109, 12620-12626.

414 14. Winkler, A.; Heintz, U.; Lindner, R.; Reinstein, J.; Shoeman, R. L.; Schlichting, I., A Ternary
415 Appa-Ppsr-DNA Complex Mediates Light Regulation of Photosynthesis-Related Gene Expression.
416 *Nature Structural & Molecular Biology* **2013**, 20, 859-867.

417 15. Jung, A.; Reinstein, J.; Domratcheva, T.; Shoeman, R. L.; Schlichting, I., Crystal Structures of
418 the Appa Bluf Domain Photoreceptor Provide Insights into Blue Light-Mediated Signal Transduction.
419 *Journal of Molecular Biology* **2006**, 362, 717-732.

420 16. Jung, A.; Domratcheva, T.; Tarutina, M.; Wu, Q.; Ko, W. H.; Shoeman, R. L.; Gomelsky, M.;
421 Gardner, K. H.; Schlichting, I., Structure of a Bacterial Bluf Photoreceptor: Insights into Blue Light-
422 Mediated Signal Transduction. *Proc. Natl. Acad. Sci. U. S. A.* **2005**, 102, 12350-12355.

423 17. Harper, S. M.; Christie, J. M.; Gardner, K. H., Disruption of the Lov-J Alpha Helix Interaction
424 Activates Phototropin Kinase Activity. *Biochemistry* **2004**, 43, 16184-16192.

425 18. Harper, S. M.; Neil, L. C.; Gardner, K. H., Structural Basis of a Phototropin Light Switch.
426 *Science* **2003**, 301, 1541-1544.

427 19. Lukacs, A.; Eker, A. P. M.; Byrdin, M.; Brettel, K.; Vos, M. H., Electron Hopping through the 15
428 Angstrom Triple Tryptophan Molecular Wire in DNA Photolyase Occurs within 30 Ps. *Journal of the*
429 *American Chemical Society* **2008**, 130, 14394-+.

430 20. Gauden, M.; van Stokkum, I. H. M.; Key, J. M.; Luhrs, D. C.; Van Grondelle, R.; Hegemann, P.;
431 Kennis, J. T. M., Hydrogen-Bond Switching through a Radical Pair Mechanism in a Flavin-Binding
432 Photoreceptor. *Proc. Natl. Acad. Sci. U. S. A.* **2006**, 103, 10895-10900.

433 21. Kennis, J. T. M.; Crosson, S.; Gauden, M.; van Stokkum, I. H. M.; Moffat, K.; van Grondelle, R.,
434 Primary Reactions of the Lov2 Domain of Phototropin, a Plant Blue-Light Photoreceptor.
435 *Biochemistry* **2003**, *42*, 3385-3392.

436 22. Kao, Y. T.; Saxena, C.; He, T. F.; Guo, L. J.; Wang, L. J.; Sancar, A.; Zhong, D. P., Ultrafast
437 Dynamics of Flavins in Five Redox States. *Journal of the American Chemical Society* **2008**, *130*, 13132-
438 13139.

439 23. Goings, J. J.; Li, P. F.; Zhu, Q. W.; Hammes-Schiffer, S., Formation of an Unusual Glutamine
440 Tautomer in a Blue Light Using Flavin Photocycle Characterizes the Light-Adapted State. *Proc. Natl. Acad. Sci. U. S. A.* **2020**, *117*, 26626-26632.

442 24. Goyal, P.; Hammes-Schiffer, S., Role of Active Site Conformational Changes in Photocycle
443 Activation of the Appa Bluf Photoreceptor. *Proc. Natl. Acad. Sci. U. S. A.* **2017**, *114*, 1480-1485.

444 25. Domratcheva, T.; Hartmann, E.; Schlichting, I.; Kottke, T., Evidence for Tautomerisation of
445 Glutamine in Bluf Blue Light Receptors by Vibrational Spectroscopy and Computational Chemistry.
446 *Scientific Reports* **2016**, *6*.

447 26. Udvarhelyi, A.; Domratcheva, T., Glutamine Rotamers in Bluf Photoreceptors: A Mechanistic
448 Reappraisal. *Journal of Physical Chemistry B* **2013**, *117*, 2888-2897.

449 27. Dittrich, M.; Freddolino, P. L.; Schulten, K., When Light Falls in Lov: A Quantum
450 Mechanical/Molecular Mechanical Study of Photoexcitation in Phot-Lov1 of Chlamydomonas
451 Reinhardtii. *Journal of Physical Chemistry B* **2005**, *109*, 13006-13013.

452 28. Konold, P. E.; Mathes, T.; Weißenborn, J.; Groot, M. L.; Hegemann, P.; Kennis, J. T. M.,
453 Unfolding of the C-Terminal α Helix in the Lov2 Photoreceptor Domain Observed by Time-Resolved
454 Vibrational Spectroscopy. *The Journal of Physical Chemistry Letters* **2016**, 3472-3476.

455 29. Alexandre, M. T. A.; Domratcheva, T.; Bonetti, C.; van Wilderen, L. J. G. W.; van Grondelle, R.;
456 Groot, M.-L.; Hellingwerf, K. J.; Kennis, J. T. M., Primary Reactions of the Lov2 Domain of Phototropin
457 Studied with Ultrafast Mid-Infrared Spectroscopy and Quantum Chemistry. *Biophysical Journal* **2009**,
458 *97*, 227-237.

459 30. Alexandre, M. T. A.; van Wilderen, L. J. G.; van Grondelle, R.; Hellingwerf, K. J.; Groot, M. L.;
460 Kennis, J. T. M., Early Steps in Blue Light Reception by Plants: An Ultrafast Mid-Infrared
461 Spectroscopic Study of the Lov2 Domain of Phototropin. *Biophysical Journal* **2005**, *88*, 509A-509A.

462 31. Iuliano, J. N., et al., Variation in Lov Photoreceptor Activation Dynamics Probed by Time-
463 Resolved Infrared Spectroscopy. *Biochemistry* **2017**.

464 32. Gil, A. A., et al., Photoactivation of the Bluf Protein Pixd Probed by the Site-Specific
465 Incorporation of Fluorotyrosine Residues. *Journal of the American Chemical Society* **2017**, *139*,
466 14638-14648.

467 33. Lukacs, A.; Haigney, A.; Brust, R.; Zhao, R. K.; Stelling, A. L.; Clark, I. P.; Towrie, M.; Greetham,
468 G. M.; Meech, S. R.; Tonge, P. J., Photoexcitation of the Blue Light Using Fad Photoreceptor Appa
469 Results in Ultrafast Changes to the Protein Matrix. *Journal of the American Chemical Society* **2011**,
470 *133*, 16893-16900.

471 34. Stelling, A. L.; Ronayne, K. L.; Nappa, J.; Tonge, P. J.; Meech, S. R., Ultrafast Structural
472 Dynamics in Bluf Domains: Transient Infrared Spectroscopy of Appa and Its Mutants. *Journal of the
473 American Chemical Society* **2007**, *129*, 15556-15564.

474 35. Lorenz-Fonfria, V. A., Infrared Difference Spectroscopy of Proteins: From Bands to Bonds.
475 *Chemical Reviews* **2020**, *120*, 3466-3576.

476 36. Frontieria, R. R.; Mathies, R. A., Femtosecond Stimulated Raman Spectroscopy. *Laser &*
477 *Photonics Reviews* **2011**, *5*, 102-113.

478 37. Kukura, P.; McCamant, D. W.; Mathies, R. A., Femtosecond Stimulated Raman Spectroscopy.
479 In *Annual Review of Physical Chemistry*, 2007; Vol. 58, pp 461-488.

480 38. Weigel, A.; Dobryakov, A.; Klaumunzer, B.; Sajadi, M.; Saalfrank, P.; Ernsting, N. P.,
481 Femtosecond Stimulated Raman Spectroscopy of Flavin after Optical Excitation. *Journal of Physical
482 Chemistry B* **2011**, *115*, 3656-3680.

483 39. Hall, C. R.; Heisler, I. A.; Jones, G. A.; Frost, J. E.; Gil, A. A.; Tonge, P. J.; Meech, S. R.,
484 Femtosecond Stimulated Raman Study of the Photoactive Flavoprotein Appa(Bluf). *Chemical Physics*
485 *Letters* **2017**, *683*, 365-369.

486 40. Andrikopoulos, P. C., et al., Femtosecond-to-Nanosecond Dynamics of Flavin
487 Mononucleotide Monitored by Stimulated Raman Spectroscopy and Simulations. *Physical Chemistry*
488 *Chemical Physics* **2020**, *22*, 6538-6552.

489 41. Iuliano, J. N., et al., Excited State Vibrations of Isotopically Labeled Fmn Free and Bound to a
490 Light-Oxygen-Voltage (Lov) Protein. *Journal of Physical Chemistry B* **2020**, *124*, 7152-7165.

491 42. Kitagawa, T.; Nishina, Y.; Kyogoku, Y.; Yamano, T.; Ohishi, N.; Takaisuzuki, A.; Yagi, K.,
492 Resonance Raman-Spectra of Carbon-13-Labeled and Nitrogen-15-Labeled Riboflavin Bound to Egg-
493 White Flavoprotein. *Biochemistry* **1979**, *18*, 1804-1808.

494 43. Copeland, R. A.; Spiro, T. G., Ultraviolet Resonance Raman-Spectroscopy of Flavin
495 Mononucleotide and Flavin Adenine-Dinucleotide. *Journal of Physical Chemistry* **1986**, *90*, 6648-
496 6654.

497 44. Quincy, T. J.; Barclay, M. S.; Caricato, M.; Elles, C. G., Probing Dynamics in Higher-Lying
498 Electronic States with Resonance-Enhanced Femtosecond Stimulated Raman Spectroscopy. *The*
499 *Journal of Physical Chemistry A* **2018**, *122*, 8308-8319.

500 45. Barclay, M. S.; Caricato, M.; Elles, C. G., Femtosecond Stimulated Raman Scattering from
501 Triplet Electronic States: Experimental and Theoretical Study of Resonance Enhancements. *Journal of*
502 *Physical Chemistry A* **2019**, *123*, 7720-7732.

503 46. Shin, K. S. K.; Zink, J. I., Quantitative Evaluation of the Relationships between Excited-State
504 Geometry and the Intensities of Fundamentals, Overtones, and Combination Bands in Resonance
505 Raman Spectra. *Inorganic Chemistry* **1989**, *28*, 4358-4366.

506 47. Tannor, D. J.; Heller, E. J., Polyatomic Raman Scattering for General Harmonic Potentials. *The*
507 *Journal of Chemical Physics* **1982**, *77*, 202-218.

508 48. Heller, E. J.; Sundberg, R.; Tannor, D., Simple Aspects of Raman Scattering. *The Journal of*
509 *Physical Chemistry* **1982**, *86*, 1822-1833.

510 49. Myers, A. B., 'Time-Dependent' Resonance Raman Theory. *Journal of Raman Spectroscopy*
511 **1997**, *28*, 389-401.

512 50. Myers Kelley, A., Resonance Raman and Resonance Hyper-Raman Intensities: Structure and
513 Dynamics of Molecular Excited States in Solution. *The Journal of Physical Chemistry A* **2008**, *112*,
514 11975-11991.

515 51. Albrecht, A. C., On the Theory of Raman Intensities. *The Journal of Chemical Physics* **1961**,
516 *34*, 1476-1484.

517 52. Heather, R.; Metiu, H., Time-Dependent Theory of Raman Scattering for Systems with
518 Several Excited Electronic States: Application to a H+3 Model System. *The Journal of Chemical*
519 *Physics* **1989**, *90*, 6903-6915.

520 53. Wang, X.; Valverde-Aguilar, G.; Weaver, M. N.; Nelsen, S. F.; Zink, J. I., Resonance Raman De-
521 Enhancement Caused by Excited State Mixed Valence. *The Journal of Physical Chemistry A* **2007**, *111*,
522 5441-5447.

523 54. Myers, A. B.; Trulson, M. O.; Mathies, R. A., Quantitation of Homogeneous and
524 Inhomogeneous Broadening Mechanisms in Trans-Stilbene Using Absolute Resonance Raman
525 Intensities. *The Journal of Chemical Physics* **1985**, *83*, 5000-5006.

526 55. Myers, A. B.; Trulson, M. O.; Pardo, J. A.; Heeremans, C.; Lugtenburg, J.; Mathies, R. A.,
527 Absolute Resonance Raman Intensities Demonstrate That the Spectral Broadening Induced by the B-
528 Ionone Ring in Retinal Is Homogeneous. *The Journal of Chemical Physics* **1986**, *84*, 633-640.

529 56. Hall, C. R.; Conyard, J.; Heisler, I. A.; Jones, G.; Frost, J.; Browne, W. R.; Feringa, B. L.; Meech,
530 S. R., Ultrafast Dynamics in Light-Driven Molecular Rotary Motors Probed by Femtosecond
531 Stimulated Raman Spectroscopy. *Journal of the American Chemical Society* **2017**, *139*, 7408-7414.

532 57. Heisler, I. A.; Moca, R.; Camargo, F. V. A.; Meech, S. R., Two-Dimensional Electronic
533 Spectroscopy Based on Conventional Optics and Fast Dual Chopper Data Acquisition. *Review of*
534 *Scientific Instruments* **2014**, *85*, 10.

535 58. Frisch, M. J., et al., Gaussian 09, Revision B.01. Wallingford CT, 2009.

536 59. Scalmani, G.; Frisch, M. J.; Mennucci, B.; Tomasi, J.; Cammi, R.; Barone, V., Geometries and
537 Properties of Excited States in the Gas Phase and in Solution: Theory and Application of a Time-
538 Dependent Density Functional Theory Polarizable Continuum Model. *The Journal of Chemical Physics*
539 **2006**, *124*, 094107.

540 60. Tomasi, J.; Mennucci, B.; Cammi, R., Quantum Mechanical Continuum Solvation Models.
541 *Chemical Reviews* **2005**, *105*, 2999-3094.

542 61. Becke, A. D., Density-Functional Thermochemistry. iii. The Role of Exact Exchange. *The*
543 *Journal of Chemical Physics* **1993**, *98*, 5648-5652.

544 62. Lee, C.; Yang, W.; Parr, R. G., Development of the Colle-Salvetti Correlation-Energy Formula
545 into a Functional of the Electron Density. *Physical Review B* **1988**, *37*, 785-789.

546 63. Wetmore, S. D.; Huang, Y., Looking Back on 90 Years of the Canadian Journal of Chemistry.
547 *Canadian Journal of Chemistry* **2019**, *97*, iii-iv.

548 64. Zenichowski, K.; Gothe, M.; Saalfrank, P., Exciting Flavins: Absorption Spectra and Spin-Orbit
549 Coupling in Light–Oxygen–Voltage (Lov) Domains. *Journal of Photochemistry and Photobiology A: Chemistry* **2007**, *190*, 290-300.

550 65. Brealey, G. J.; Kasha, M., The Role of Hydrogen Bonding in the N- Pi-Star Blue-Shift
551 Phenomenon. *Journal of the American Chemical Society* **1955**, *77*, 4462-4468.

552 66. Lu, T.; Chen, F., Multiwfn: A Multifunctional Wavefunction Analyzer. *Journal of*
553 *Computational Chemistry* **2012**, *33*, 580-592.

554 67. Kucharski, S. A.; Włoch, M.; Musiał, M.; Bartlett, R. J., Coupled-Cluster Theory for Excited
555 Electronic States: The Full Equation-of-Motion Coupled-Cluster Single, Double, and Triple Excitation
556 Method. *The Journal of Chemical Physics* **2001**, *115*, 8263-8266.

557 68. Korona, T.; Werner, H.-J., Local Treatment of Electron Excitations in the Eom-Ccsd Method.
558 *The Journal of Chemical Physics* **2003**, *118*, 3006-3019.

559 69. Rishi, V.; Perera, A.; Nooijen, M.; Bartlett, R. J., Excited States from Modified Coupled Cluster
560 Methods: Are They Any Better Than Eom Ccsd? *The Journal of Chemical Physics* **2017**, *146*, 144104.

561 70. NIST Nist Standard Reference Database Number 101. 2020;
562 [Https://Cccbdb.Nist.Gov/Vibscalejust.Asp](https://Cccbdb.Nist.Gov/Vibscalejust.Asp). <https://cccbdb.nist.gov/vibscalejust.asp> (accessed 4-13-
563 21).

564 71. Schmidt, J.; Coudron, P.; Thompson, A. W.; Watters, K. L.; McFarland, J. T., Hydrogen
565 Bonding between Flavin and Protein: A Resonance Raman Study. *Biochemistry* **1983**, *22*, 76-84.

566 72. Petrenko, T.; Neese, F., Analysis and Prediction of Absorption Band Shapes, Fluorescence
567 Band Shapes, Resonance Raman Intensities, and Excitation Profiles Using the Time-Dependent
568 Theory of Electronic Spectroscopy. *The Journal of Chemical Physics* **2007**, *127*, 164319.

569 73. Kim, H.; Kosuda, K. M.; Van Duyne, R. P.; Stair, P. C., Resonance Raman and Surface- and Tip-
570 Enhanced Raman Spectroscopy Methods to Study Solid Catalysts and Heterogeneous Catalytic
571 Reactions. *Chemical Society Reviews* **2010**, *39*, 4820-4844.

573

574

